

# Feedforward selective fixed-filter active noise control : algorithm and implementation

Shi, Dongyuan; Gan, Woon-Seng; Lam, Bhan; Wen, Shulin

2020

Shi, D., Gan, W.-S., Lam, B., & Wen, S. (2020). Feedforward selective fixed-filter active noise control : algorithm and implementation. *IEEE/ACM Transactions on Audio, Speech, and Language Processing*, 28, 1479-1492. doi:10.1109/TASLP.2020.2989582

<https://hdl.handle.net/10356/142040>

<https://doi.org/10.1109/TASLP.2020.2989582>

---

© 2020 IEEE. Personal use of this material is permitted. Permission from IEEE must be obtained for all other uses, in any current or future media, including reprinting/republishing this material for advertising or promotional purposes, creating new collective works, for resale or redistribution to servers or lists, or reuse of any copyrighted component of this work in other works. The published version is available at:  
<https://doi.org/10.1109/TASLP.2020.2989582>

*Downloaded on 19 Sep 2022 10:51:19 SGT*

# Feedforward Selective Fixed-filter Active Noise Control: Algorithm and Implementation

Dongyuan Shi, *Student Member, IEEE*, Woon-Seng Gan, *Senior Member, IEEE*,  
Bhan Lam, *Student Member, IEEE*, and Shulin Wen

**Abstract**—Conventional real-time active noise control (ANC) usually employs the adaptive filtered-x least mean square (FxLMS) algorithm to approach optimum coefficients for the control filter. However, lengthy training is usually required, and the perceived noise reduction is not immediately realized. Motivated by the practical implementation, we propose a selective fixed-filter active noise control (SFANC) algorithm, which selects a pre-trained control filter to attenuate the detected primary noise rapidly. On top of improved robustness, the complexity analysis reveals that SFANC appears to be more efficient. The SFANC algorithm chooses the most suitable control filter based on the frequency-band-match approach implemented in a partitioned frequency-domain filter. Through simulations, SFANC is shown to exhibit a satisfactory response time and steady-state noise reduction performance, even for time-varying noise and real non-stationary disturbance.

**Index Terms**—Active Noise Control, Selective fixed-filter active noise control, Frequency-domain filtering, Filtered-x Least Mean Square

## I. INTRODUCTION

ACTIVE noise control (ANC) generally employs a secondary source to generate ‘anti-noise’ wave that destructively suppresses the unwanted noise in the listening environment. The underlying signal processing mechanism behind ANC is the filtered-x least mean square (FxLMS) algorithm. FxLMS is an adaptive algorithm that updates the coefficients of a control filter in real-time intending to create an anti-noise signal, which matches the primary noise in space and time at the desired location [1]–[3]. Although ANC is commonly used in noise-cancelling headsets [4], [5] and modern automobiles [6]–[9], its application in larger three-dimensional spaces has been limited [10], [11]. To effectively attenuate broadband noise in a large space, multichannel ANC with long control filters and high sample rate are usually required [12]–[14]. In these multichannel implementations, however, high-performance processors, such as multi-core DSP processors, FPGAs [15], [16], or GPUs [17] are required, which undoubtedly increases implementation costs and complicates the programming effort. These processing limitations, thus, undermine its potential applications (e.g., in facade openings [11], [18], large dimension ducts or room interiors, active noise barriers [19]).

There are many approaches to alleviate the computational burden of ANC systems [20], [21]. One such solution is

DongYuan Shi, Woon-Seng Gan, Bhan Lam, and Shulin Wen are working in the School of Electrical and Electronic Engineering at the Nanyang Technological University, Singapore. (e-mail: DSHI003@e.ntu.edu.sg, ews-gan@ntu.edu.sg, bhanlam@ntu.edu.sg, and alicia.wen@ntu.edu.sg).

the fixed-filter approach, which is widely adopted due to its simplicity and robustness [22], [23]. In this approach, the coefficients of the control filter are first pre-trained for different ANC setups, and subsequently, these trained (fixed) control filter coefficients can be deployed in the actual operation using low-cost analog and digital processing units [24]. A point in case is exemplified by the ANC headsets, which usually employ analog filters by pre-tuning the gain and phase response to handle different types of noise environments [25], [26]. However, this approach is optimized for a limited range of noise types, which could result in mediocre noise reduction performance.

Hence, we propose a practical, computationally-efficient strategy to adapt to the different primary noise types. This approach will henceforth be known as selective fixed-filter active noise control (SFANC). The SFANC algorithm adopts a frequency-band-match approach to match the incoming noise frequency patterns with the spectrum of the control filter. The pre-trained control filter that matches the primary noise signature will be selected as the control filter for the ANC system. In this way, the control system can achieve a satisfactory noise reduction performance, without requiring high computational complexity. Moreover, due to the absence of feedback [27], SFANC exhibits arguably high robustness even for the nonstationary disturbances.

This paper is organized as follows. Section II introduces the concept of SFANC. Next, an outline of the frequency-band-match method that is used to select the control filter is detailed in Section III. Based on the frequency-band-match selection method, Section IV describes the implementation of the SFANC algorithm, and Section V analyzes the computational complexity of the proposed algorithm. To verify the effectiveness of the proposed algorithm, a series of numerical simulations were detailed in Section VI. The final section concludes the paper.

## II. SELECTIVE FIXED-FILTER ACTIVE NOISE CONTROL APPROACH

The primary and secondary paths barely vary over time in many realistic operating environments, such as in a car cabin or an air duct [28]. For simplicity, we assume that the impulse responses of these acoustic paths are time-invariant in the following discussions. Hence, we pre-train the control filter coefficients for a specific acoustic path in a preliminary stage to attenuate a specific primary noise. This describes the aforementioned fixed-filter method, which avoids

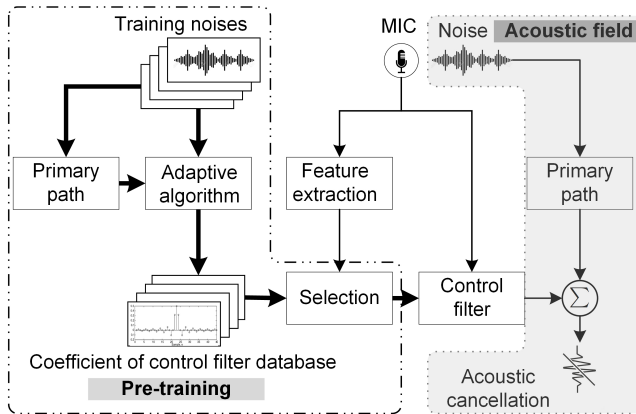


Fig. 1. The processing block of the SFANC method, which features the first stage of deriving a set of control filters based on commonly encountered noise types and noise paths. Subsequently, selective algorithm extracts the closest control filter to filter out the actual noise in real-time.

the adaptive updating during the control stage. However, each fixed filter only works well for a specific primary noise, and thus, variation in the primary noise will unquestionably affect the noise cancellation performance. To improve the noise reduction performance of the fixed filter to accommodate different primary noise types, the selective fixed-filter active noise control (SFANC) approach is proposed [22], [23]. The SFANC approach operates in two stages: (1) an offline pre-training stage where a database of control filters are trained before implementation, and (2) an online control stage where the disturbance is mitigated by the most appropriate control filter, as shown in Fig. 1.

#### A. Offline pre-training stage of control filters

Compared to the conventional ANC method, SFANC involves a preliminary training stage, as shown in Fig. 1. In this stage, a series of measured or synthesized noises sources are utilized for training. The training noises are firstly filtered by real or measured primary paths, which creates the corresponding disturbances. Subsequently, the adaptive algorithm utilizes both the training noises and disturbances to obtain corresponding sets of optimal filters.

#### B. Online control: Feature extraction and control filter selection

In the online control stage, features of the detected noise are firstly extracted, as shown in Fig. 1. These extracted features, such as the amplitude, frequency, or phase, should be unique characteristics that can distinguish noise types up to the required accuracy. Subsequently, the SFANC system selects the control filter from the database based on the extracted features.

Hence, it becomes apparent that an inappropriately chosen control filter produces inferior noise reduction performance compared to the conventional FxLMS algorithm. Popular machine learning or deep learning methods, such as the convolutional neural network (CNN) [29], can possibly classify

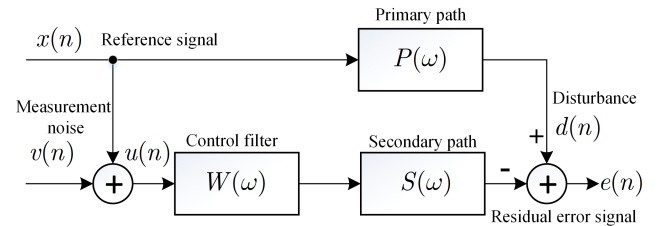


Fig. 2. Block diagram of single channel feedforward ANC. The primary noise disturbance is denoted as  $d(k)$  and the residual error signal  $e(k)$  is acoustically measured from microphone at the control region.

the incoming primary noise to match the most appropriate control filter. Nevertheless, since these computationally-intensive classification methods increase the overall latency of the SFANC online control stage, its practicality is undermined. To overcome this problem, the following sections use the frequency-band-match method for filter selection and propose an efficient SFANC algorithm based on this method.

Once the control filter is selected, the SFANC system functions as a fixed filter. It processes the primary noise acquired by the reference microphone and generates an anti-noise signal to cancel the disturbance, as illustrated in Fig. 1. In contrast to the conventional adaptive ANC method, the absence of a feedback signal [30] from the error microphone in SFANC minimizes the risk of algorithm divergence.

### III. FREQUENCY-BAND-MATCH ALGORITHM FOR SFANC

As mentioned in the previous section, the challenge of the SFANC system is the selection of a suitable control filter for the specific type of primary noise. This section introduces a frequency-band-match approach, which chooses the pre-trained filter based on the similarity of the spectral contents between the training signal and the actual primary noise. Here, the spectral content only involves the central frequency and bandwidth of the frequency band. Hence, the spectral contents of the primary noise become the critical feature for filter selection.

Figure 2 shows a single channel feedforward ANC system, where  $P(\omega)$  and  $S(\omega)$  represent the transfer function of the primary path and the secondary path, respectively, and  $W(\omega)$  denotes the transfer function of the control filter. For simplicity, the reference signal is assumed to be directly acquired from the noise source.

In the training phase, a broadband training signal  $X_0(\omega)$  is input as a reference signal

$$X_0(\omega) = T_0(\omega) \cdot \text{rect}\left(\frac{\omega - \omega_0}{2B_0}\right) \quad (1)$$

where  $T_0(\omega)$  is a conjugate symmetric function with respect to frequency  $\omega$  [31].  $\omega_0$  and  $B_0$  are the central frequency and bandwidth of the training signal, respectively. The rectangular function in (1) is given by

$$\text{rect}\left(\frac{\omega - \omega_0}{2B_0}\right) = \begin{cases} 1 & |\omega| \in [\omega_0 - B_0, \omega_0 + B_0] \\ 0 & \text{otherwise.} \end{cases} \quad (2)$$

The filtered reference signal is given by

$$r_0(k) = x_0(k) * s(k) \quad (3)$$

where  $*$  stands for the linear convolution operation.  $x_0(k)$  and  $s(k)$  represent the training signal and the impulse response of the secondary path, respectively. Hence, the power spectral density (PSD) of the filtered reference signal is written as

$$S_{r_0}(\omega) = S_{x_0}(\omega)|S(\omega)|^2 \cdot \text{rect}\left(\frac{\omega - \omega_0}{2B_0}\right) \quad (4)$$

where  $S(\omega)$  denotes the transfer function of the secondary path, and the PSD of the training signal is given by

$$S_{x_0} = \mathbb{E}[X_0(\omega)X_0^*(\omega)] \quad (5)$$

where  $\mathbb{E}[\cdot]$  is the expectation operator. The cross-spectral density of the filtered reference  $r_0(k)$  and the disturbance  $d(k)$  is expressed as

$$S_{d_0 r_0}(\omega) = S_{x_0}(\omega)P(\omega)S^*(\omega) \cdot \text{rect}\left(\frac{\omega - \omega_0}{2B_0}\right). \quad (6)$$

According to [33], we can obtain the optimal control filter for the training signal at  $\omega \in [\omega_0 - B_0, \omega_0 + B_0]$  by

$$W_{\text{opt}}^0(\omega) = \frac{S_{d_0 r_0}(\omega)}{S_{r_0}(\omega)} = \frac{P(\omega)}{S(\omega)}. \quad (7)$$

A recursive algorithm, such as the FxLMS algorithm, can be used to compute  $W_{\text{opt}}^0(\omega)$  outside the frequency range of interest (i.e.,  $|\omega| \in [0, \omega_0 - B_0] \cup (\omega_0 + B_0, \pi]$ ). If the training signal is  $X_0(\omega) = 0$  ( $|\omega| \in [0, \omega_0 - B_0] \cup (\omega_0 + B_0, \pi]$ ), then its optimal control filter (derivation in Appendix A) is

$$W_{\text{opt}}^0(\omega) = 0, \quad |\omega| \in [0, \omega_0 - B_0] \cup (\omega_0 + B_0, \pi]. \quad (8)$$

By combining (7) and (8), the optimal control filter for the training signal can be rewritten as

$$W_{\text{opt}}^0(\omega) = \frac{S_{d_0 r_0}(\omega)}{S_{r_0}(\omega)} \cdot \text{rect}\left(\frac{\omega - \omega_0}{2B_0}\right) = \frac{P(\omega)}{S(\omega)} \cdot \text{rect}\left(\frac{\omega - \omega_0}{2B_0}\right). \quad (9)$$

In the control stage, the primary noise is assumed to be a broadband noise with the central frequency  $\omega_1$  and bandwidth  $B_1$

$$X_1(\omega) = T_1(\omega) \cdot \text{rect}\left(\frac{\omega - \omega_1}{2B_1}\right) \quad (10)$$

where  $T_1(\omega)$  is a conjugate symmetric function with respect to frequency  $\omega$ . The rectangular function in (10) is given by

$$\text{rect}\left(\frac{\omega - \omega_1}{2B_1}\right) = \begin{cases} 1 & |\omega| \in [\omega_1 - B_1, \omega_1 + B_1] \\ 0 & \text{otherwise.} \end{cases} \quad (11)$$

The optimal control filter with primary noise  $X_1(\omega)$  is derived as

$$W_{\text{opt}}^1(\omega) = \frac{S_{d_1 r_1}(\omega)}{S_{r_1}(\omega)} \cdot \text{rect}\left(\frac{\omega - \omega_1}{2B_1}\right) = \frac{P(\omega)}{S(\omega)} \cdot \text{rect}\left(\frac{\omega - \omega_1}{2B_1}\right). \quad (12)$$

The reference signal  $u(k)$ , as illustrated in Fig. 2, is given by

$$u(k) = x_1(k) + v(k) \quad (13)$$

where  $v(k)$  denotes a white Gaussian noise  $v(k) \sim N(0, N_0/2)$ , which represents the quantization noise, measurement noise on the reference sensor, or electronic component interference. If we apply  $W_{\text{opt}}^0(\omega)$  as the control filter in Fig. 2 to attenuate the primary noise, its error signal can be rewritten as

$$e(k) = d_1(k) - [x_1(k) + v(k)] * w_{\text{opt}}^0(k) * s(k) \quad (14)$$

where  $d_1(k)$  denotes the disturbance, and  $w_{\text{opt}}^0(k)$  represents the impulse response of the optimal control filter in the pre-training stage. The filtered reference signal is  $r_1(k) = x_1(k) * s(k)$ .

To simplify the analysis, we assume that  $\omega_0 = \omega_1$  and  $B_1 \leq B_0$ . As detailed in Appendix B, the PSD of the error signal in (14) is given by

$$S_e(\omega) = S_e(\omega)_{\min} \cdot \text{rect}\left(\frac{\omega - \omega_0}{2B_1}\right) + \frac{N_0}{2}|P(\omega)|^2 \left[ \text{rect}\left(\frac{\omega - \omega_0}{2B_0}\right) - \text{rect}\left(\frac{\omega - \omega_0}{2B_1}\right) \right] \quad (15)$$

where

$$S_e(\omega)_{\min} = S_{d_1}(\omega) - \frac{|S_{d_1 r_1}(\omega)|^2}{S_{r_1}(\omega)} + \frac{N_0}{2}|P(\omega)|^2 \quad (16)$$

and  $S_{d_1}(\omega) = \mathbb{E}[D_1^*(\omega)D_1(\omega)]$ . Here,  $S_e(\omega)_{\min}$  is the PSD of the error signal when the control filter arrives at the optimal solution  $W_{\text{opt}}^1(\omega)$  [33]. If the primary path is approximated as a delay with unit gain, the mean square error (MSE) is derived by integrating (15)

$$\begin{aligned} \mathbb{E}[e^2(k)] &= \frac{1}{2\pi} \int_{-\pi}^{\pi} S_e(\omega) d\omega \\ &= J_{\min} + \frac{N_0}{2\pi} (B_0 - B_1) \end{aligned} \quad (17)$$

where

$$J_{\min} = \frac{1}{2\pi} \int_{-\pi}^{\pi} S_e(\omega)_{\min} d\omega \quad (18)$$

which is the minimal mean square error (MMSE) of the Wiener-Hopf solution [33], [34]. In (17), if the bandwidth  $B_0$  equals  $B_1$ , the MMSE of SFANC is the same as that of the FxLMS algorithm.

It is worth noting that the same result can be observed even when the primary path is not a unit gain. Therefore, if the training signal of the control filter in the SFANC algorithm has the same central frequency and bandwidth as the primary noise, the SFANC algorithm can achieve the same noise reduction level as the FxLMS algorithm.

#### IV. PROPOSED SELECTIVE FIXED-FILTER ACTIVE NOISE CONTROL ALGORITHM

In this section, we describe the proposed selective fixed-filter noise control (SFANC) algorithm, which uses the frequency-band-match method to perform the control filter selection for different primary noises. SFANC adopts the comb-partitioning filter structure, and the coefficients of the control filters are obtained through a modified comb-partitioning frequency-domain adaptive filter (comb-PFDAF) [35], [36]

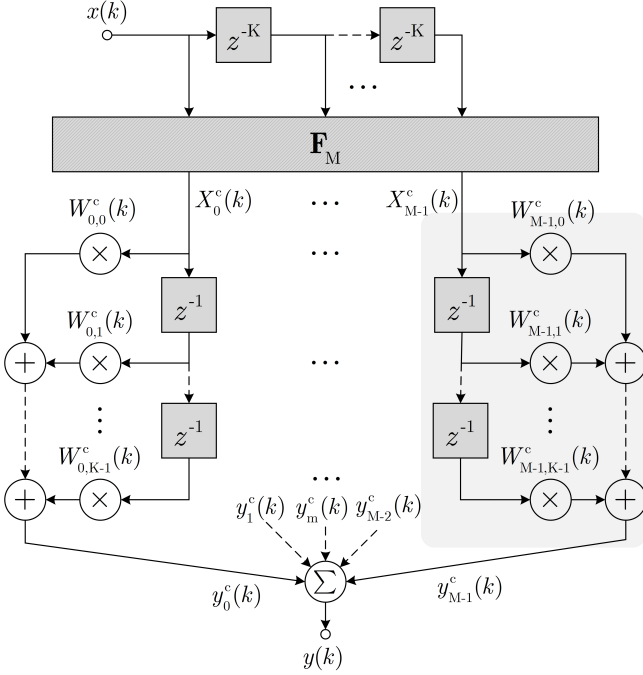


Fig. 3. Partitioned structure of the filter in  $K$  combs. The input signal is down-sampled at  $K$  times and then finishes the FFT operation to generate  $M$  frequency bins. The frequency bins are input to the  $M$  filter branches, and the summation of these branches is the output of the partitioned filter.

algorithm. In comparison to other frequency-domain adaptive filters (PFDAF) [37]–[41], comb-PFDAF significantly reduces the computational complexity of the Fourier transformation in the algorithm [35], [42].

It is worth noting that in many ANC applications, the reference sensor is used to acquire as much information about the primary source as possible. Hence, it is reasonable to assume that the reference signal has the same central frequency and bandwidth as the primary noise.

#### A. Pre-training stage of the control filters

In the pre-training stage, a series of synthesized broadband signals are utilized as the primary noise to train a database of control filters. These broadband signals are created by passing white Gaussian noise through band-pass filters with different frequency bands. The comb-PFDAF algorithm is applied to train the control filters due to its reduced computational complexity in extracting the frequency spectrum of the reference signal in an adaptive manner.

In the section, we consider a control filter with a length of  $N$ . According to the comb-partitioning method, we split the impulse response of the control filter into  $K$  combs. The length of each comb is equal to  $M = N/K$ , where  $K = 1, 2, \dots, N$ . A DFT of length  $M$  is needed in the partitioned structure, as shown in Fig. 3.

In the partitioned filter, the input signal  $x(k)$ , at the  $k$ th iteration, is decimated by a factor of  $K$  to form the comb-partitioned reference signal given by

$$\mathbf{x}^c(k) = [x(k), x(k - K), \dots, x(k - (M - 1)K)]^T \quad (19)$$

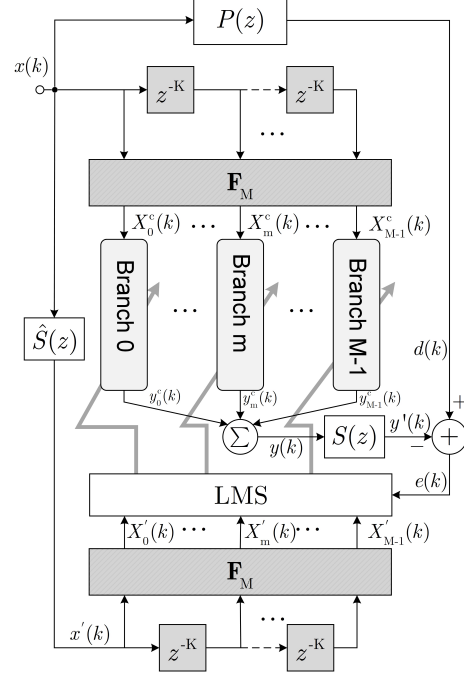


Fig. 4. Block diagram of the filtered reference comb-partitioning frequency domain adaptive filter (FxCFDAF), which adopts the filtered reference signal based on the secondary path estimate  $\hat{S}(z)$ .

and its Fourier transform is

$$\mathbf{X}(k) = \mathbf{F}_M \mathbf{x}^c(k) = [X_0^c(k), X_1^c(k), \dots, X_{M-1}^c(k)]^T \quad (20)$$

where  $\mathbf{F}_M \in \mathbb{C}^{M \times M}$  denotes the Fourier transform matrix given by

$$\mathbf{F}_M = \left( e^{-\frac{2\pi \cdot j \cdot i}{M}} / \sqrt{M} \right)_{i,j=0,\dots,M-1} \quad (21)$$

It is worth noting that the value of  $M$  decides the frequency resolutions of the reference signal but does not influence the result of the signal filtering. Hence, it should be large enough to express the spectral contents of the reference signal. The output of the  $m$ th branch in the control filter, as shown in Fig. 3, is expressed as

$$y_m^c(k) = [\mathbf{W}_m^c(k)]^T \mathbf{X}_m^c(k) = \sum_{i=0}^{K-1} W_{m,i}^c(k) X_m^c(k-i) \quad (22)$$

where

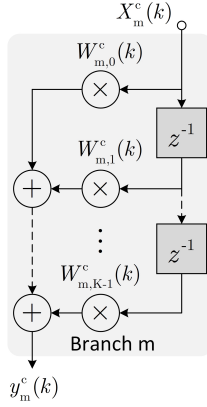
$$\begin{aligned} \mathbf{W}_m^c(k) &= [W_{m,0}^c(k), W_{m,1}^c(k), \dots, W_{m,K-1}^c(k)]^T \\ \mathbf{X}_m^c(k) &= [X_m^c(k), X_m^c(k-1), \dots, X_m^c(k-K+1)]^T \end{aligned} \quad (23)$$

$$m = 0, 1, \dots, M-1.$$

The output signal of the control filter is obtained from the summation of all branches as

$$y(k) = \sum_{m=0}^{M-1} y_m(k). \quad (24)$$

To recursively update the coefficient of the control filter, we propose the filtered reference comb-partitioning frequency domain adaptive filter (FxCFDAF), as illustrated in Fig. 4

Fig. 5. Block diagram of the  $m$ th branch in FxCFDAF algorithm.

and Fig. 5. For each weight vector  $\mathbf{W}_m^c(k)$ , as proven in Appendix C, its update equation is given by

$$\mathbf{W}_m^c(k+1) = \mathbf{W}_m^c(k) + \mu e(k) \mathbf{X}'_m(k) \quad (25)$$

where  $\mu$  denotes the step size, and

$$\mathbf{X}'_m(k) = [X'_m(k), X'_m(k-1), \dots, X'_m(k-K+1)]^T \quad (26)$$

$X'_m(k)$  represents the  $m$ th frequency bin in the Fourier transform of the filtered reference given by

$$x'(k) = \hat{s}(k) * x(k) \quad (27)$$

where  $\hat{s}(k)$  denotes the impulse response of the secondary path estimate.

To obtain (26), as shown in Fig. 4, the filtered reference signal is first partitioned to  $K$  combs as

$$\mathbf{x}_f^c(k) = [x'(k), x'(k-K), \dots, x'(k-(M-1)K)]^T \quad (28)$$

and its Fourier transform is calculated by

$$\begin{aligned} \mathbf{X}'_f(k) &= \mathbf{F}_M \mathbf{x}_f^c(k) \\ &= [X'_0(k), X'_1(k), \dots, X'_{M-1}(k)]^T. \end{aligned} \quad (29)$$

By staking the  $m$ th element (frequency bin) of (29) from iteration  $k$  to  $k-K+1$ , we arrive at (26).

After the coefficients of control filters for different primary noises are obtained, they are stored into a control filter library (or database), as shown in Fig. 6. In order to generate a unique index or an address for different control filters, we first estimate the power spectral density of the corresponding reference signal  $X(k)$  by accumulating its fast Fourier transform (FFT) result of each  $L$  iterations [43]

$$\mathbf{S}_x = \left[ \sum_{l=0}^{L-1} \|X_1^c(k-l)\|^2, \dots, \sum_{l=0}^{L-1} \|X_{M/2}^c(k-l)\|^2 \right]^T \quad (30)$$

Then, a threshold is derived by averaging of the minimum and maximum elements ( $S_{\min}$  and  $S_{\max}$ ) of the vector  $\mathbf{S}_x$  in (30)

$$V_{\text{thr}} = \frac{S_{\min} + S_{\max}}{2}. \quad (31)$$

It is compared with the elements of the vector  $\mathbf{S}_x$ , which results in a bit vector as

$$A = [a_1, \dots, a_i, \dots, a_{M/2}]^T \in \mathbb{R}^{M/2 \times 1} \quad (32)$$

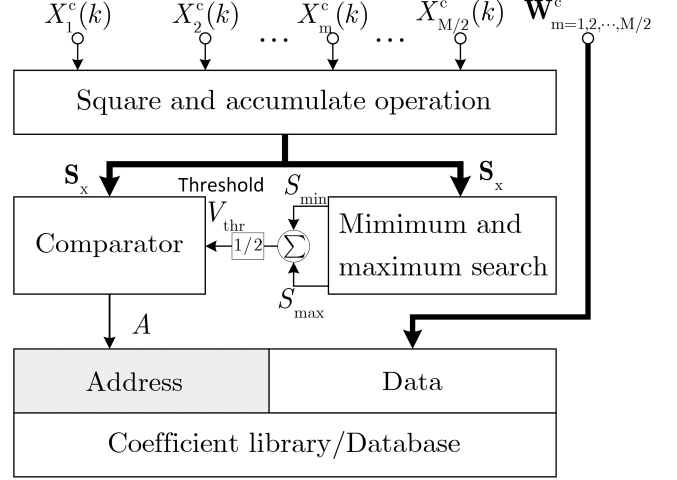


Fig. 6. The construction of coefficient library, which is used to store the pre-trained filters in training stage. The approximate power spectrum  $\mathbf{S}_x$  is used to create a bit array  $A$  as the address in the library for storing the corresponding control filter coefficients.

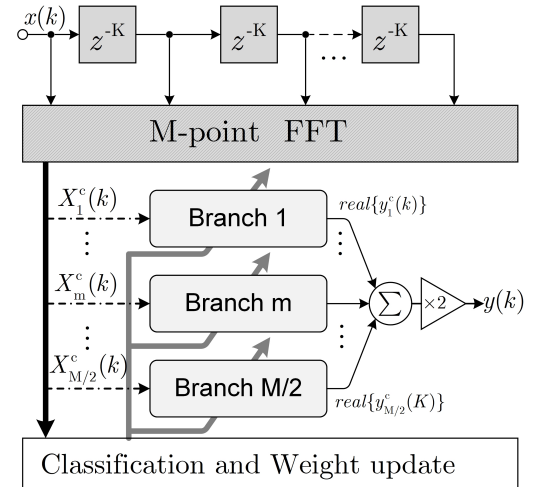


Fig. 7. Overall block diagram of the SFANC algorithm. It composed of three parts: (1). the FFT transform part of the partitioned reference signal, (2).  $M/2$  frequency filter branches, and (3). the noise classification and filter weight update part.

where

$$a_i = \begin{cases} 0, & S_{x,i} < V_{\text{thr}} \\ 1, & S_{x,i} \geq V_{\text{thr}} \end{cases} \quad (33)$$

$S_{x,i}$  represents the  $i$ th element of  $\mathbf{S}_x$ . Finally,  $A$  is utilized as the index or address of the corresponding control filter, as illustrated in Fig. 6.

### B. Selective fixed-filter active noise control algorithm

The online control stage of the selective fixed-filter active noise control (SFANC) algorithm replaces the adaptive update process of the FxCFDAF algorithm with classification and weight update based on frequency-band-match method. In the algorithm, the partitioned reference signal is still decimated from the reference signal  $X(k)$  by a factor of  $K$ , as shown in Fig. 7. In this way, the computations in the FFT of SFANC

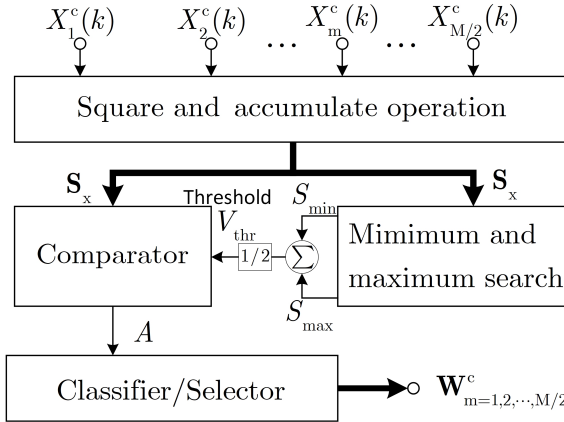


Fig. 8. The classification and weight update part in SFANC. The bit vector  $A$  created from the approximate power spectrum  $S_x$  that is utilized as the index or address to fetch the corresponding control filter for the specific primary noise.

reduces by  $K$  times, compared with performing the Fourier transform on the reference signal.

Furthermore, since the output signal of the control filter is a real signal, its frequency spectrum is conjugate symmetric. Moreover, ANC does not handle the DC component (or zero-frequency bin) of the reference signal, and thus,  $y_0^c(k) = [\mathbf{W}_0^c(k)]^T \mathbf{X}_0^c(k) = 0$ . Therefore, the output signal is expressed as

$$y(k) = 2 \sum_{m=1}^{M/2} \text{real}\{y_m^c(k)\} \quad (34)$$

where  $M$  is an even number, and  $\text{real}\{\cdot\}$  denotes the real part of a complex number.

The online part of SFANC adopts the frequency-band-match for classification, and updates the coefficients of the control filter, every  $L$  iterations. The block diagram of the classification and weight update is illustrated in Fig. 8. This unit estimates the power spectral density (PSD) of the reference in (30) and obtains the index or address  $A$  in (31). Subsequently, it fetches the pre-trained filter in the library corresponding to the index  $A$  and updates the control filter in the online control stage.

Hence, for online control, SFANC replaces the real-time adaptive update progress with classification and weight update process. The latter accomplishes one calculation in  $L$  iterations and thus, reduces the computational complexity per iteration compared to the conventional FdAF algorithm, especially for multichannel ANC applications. However, a bit vector  $A$  with a long dimension requires that the system stores a considerable number of control filters. For instance, a  $A$  vector with 16 bit elements can represent 65,536 different control filters, which are impractical to be obtained by experiments. In contrast, if we shorten the dimension of the  $A$  vector, the frequency resolution of the SFANC will decrease, which worsens the noise reduction performance of the algorithm.

Therefore, in the spirit of practicality, the classifier should select the most appropriate control filter based on similarity to input  $A$ , as shown in Fig. 8 and further detailed in Fig. 9. In its first layer of the classifier, the AND-distance network

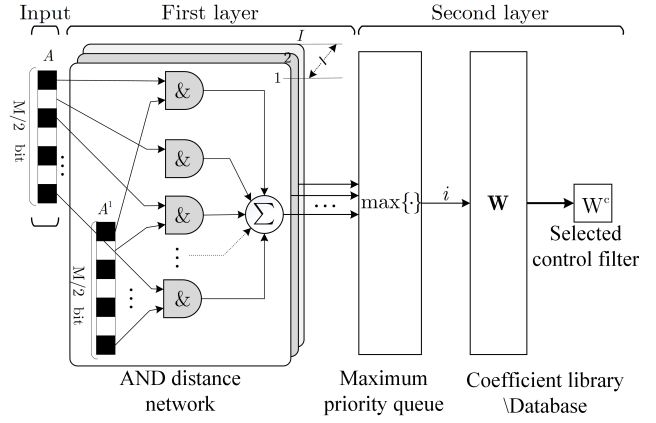


Fig. 9. Implementation architecture of the modified classifier. The index  $A$  created from the reference signal is input into the classifier. The first layer computes the binary distance or similarity between input  $A$  and the indexes of all the stored pre-trained filters ( $I$  pre-trained filters stored in the coefficient library), where ‘&’ stands for the logic AND operation. The index, which owns the maximum similarity ratio with the input  $A$ , is used to fetch the corresponding filter in the second layer.

will calculate the similarity value between the input bit vector  $A$  and the indices of all pre-trained filters.  $d_i$  represents the similarity value that equates to the number of positive comparisons (logic one) in  $A$  and  $A^i$ , where  $A^i$  indicates the address of the  $i$ th pre-trained filter. Hence, a large similarity value indicates a larger bit-for-bit similarity. Subsequently, the maximum priority queue outputs the index  $i$  with largest similarity index  $d_i$ . The corresponding  $i$ th control filter, which is obtained in the preliminary stage by (25), will be chosen as the current control filter. It is worth noting that the order of the addresses or indexes in the first layer is arranged in ascending bandwidth of the corresponding training noise. This similarity value is thus equivalent to the binary distance [44], [45] defined in Appendix D, which indirectly represents the similarity (or closeness) of the input noise spectral contents to the training noise. Based on the above mechanism, this selector can choose a pre-trained control filter, whose training noise has the most similar spectral components to the primary noise.

From Fig. 9, it is observed that the classifier only contains several AND gates and accumulators, which consumes minimal resources in the processor.

## V. COMPUTATIONAL COMPLEXITY ANALYSIS

The most time-consuming operations in a digital signal processing (DSP) algorithm are its multiplication and addition operations. Hence, in this section, we analyze the computational complexity, in terms of the multiplication and addition operations of the SFANC algorithm in comparison with the other FxLMS based algorithms.

We consider a SFANC algorithm with  $N$  coefficients and  $K$  combs. First, it consumes  $\frac{3N}{2K} \log_2 \frac{N}{K}$  real multiplications and  $\frac{2N}{K} \log_2 \frac{N}{K}$  real additions to complete the Fourier transform in (20). Subsequently, the control filter unit in (34) operates with  $N$  multiplications and  $N - 1$  additions. To compute the power spectrum, the algorithm uses  $\frac{2N}{K}$  multiplications

TABLE I  
THE NUMBER OF ADDITIONS AND MULTIPLICATIONS USED IN FxLMS,  
FDAF, SFANC ALGORITHMS, WHEN THE LENGTH OF THE CONTROL  
FILTER IS 1024.

Algorithm	Real multiplications	Real additions
FxLMS	3073	2037
FDAF	6624	5540
SFANC	1392	1312

and  $\frac{2N}{K}$  additions. Moreover, the classifier runs in parallel with the power spectral density estimation and takes  $I$  (the number of the pre-trained filters in the library) iterations to complete the classification, only consuming one addition in each iteration. Therefore, the computational complexity of SFANC is obtained as

$$\begin{cases} \Theta_{\text{Multiplication}} &= \frac{3N}{2K} \log_2 \frac{N}{K} + N + \frac{2N}{K} \\ \Theta_{\text{Addition}} &= \frac{2N}{K} \log_2 \frac{N}{K} + N + \frac{2N}{K} \end{cases} \quad (35)$$

In contrast, the FDAF algorithm uses  $\frac{2N}{K} \log_2 \frac{N}{K} + 6N$  multiplications and  $\frac{4N}{K} \log_2 \frac{N}{K} + 5N - 3$  additions in each iteration, where the length of the secondary path estimate is assumed to be  $N$ .

For example, we assume that the length of the control filter in FxLMS, FDAF, and SFANC is  $N = 1024$ , and the secondary path estimate also has  $N = 1024$  taps. The number of combs in FDAF and SFANC is equal to  $K = 16$ . The addition and multiplication usages per iteration in these three algorithms are summarized in Table I. The comparison result suggests that the SFANC algorithm has a distinct advantage in alleviating the computation load in practical real-time active control.

However, compared to the conventional adaptive algorithm, the proposed algorithm requires more memory to store the coefficients. If we assume that the coefficient is expressed in a single-precision format, SFANC will consume  $4I \times K$  bytes memory for the storage of the coefficient library. Fortunately, this library can be stored in an external memory device, such as NAND flash, which usually has a large memory size. Furthermore, the weight update part requires  $M + 1$  comparisons to obtain the bit vector every  $L$  iterations, and the classifier also needs to finish  $I$  comparisons for the  $\max\{\cdot\}$  operation during  $I$  iterations. Hence, the algorithm accomplishes  $1 + (M+1)/L$  comparisons and  $M/2$  logical AND operations besides the additions and multiplications at each iteration.

## VI. NUMERICAL SIMULATION RESULTS

To evaluate the SFANC performance and compare its performance with the conventional FxLMS algorithm, we carry out simulations of ANC control problem at a sampling rate of 10 kHz. The primary and secondary paths are chosen as a band-pass filter and a low pass filter, respectively, and their magnitude and phase responses are shown in Fig. 10.

### A. Noise reduction as a function of similarity

In Simulation A, the primary noise is set to broadband noise (750 to 1250 Hz). A series of pre-trained filters are chosen to control the noise. The training signals of these filters

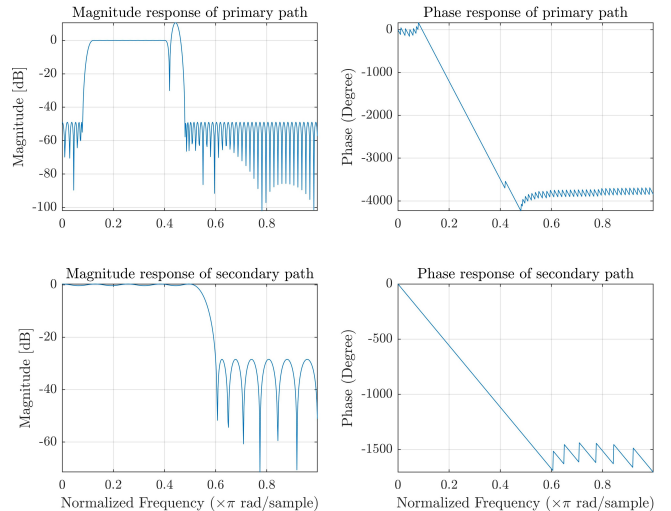


Fig. 10. Frequency and phase responses of the primary (upper row) and secondary (lower row) paths.

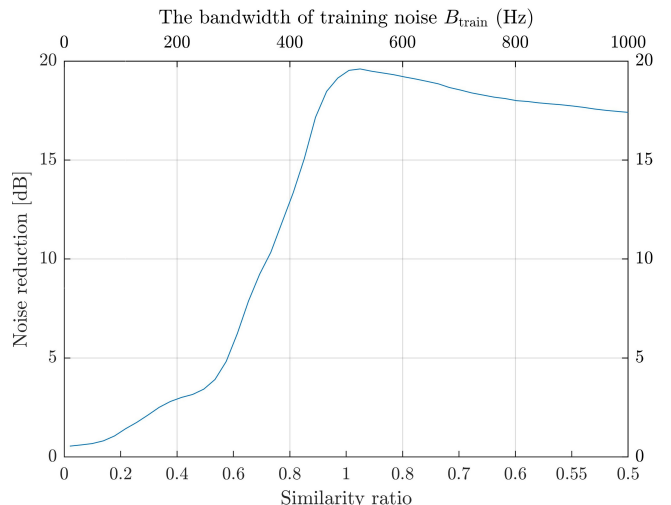


Fig. 11. Noise reduction as a function of similarity ratios and the bandwidth of the training noise  $B_{\text{train}}$  in simulation A, where the bandwidth of the primary noise  $B_{\text{primary}}$  is set to 500 Hz. The noise reduction peaks as the similarity ratio approaches 1.

had different frequency bandwidths (from 10 to 1000 Hz) with the same central frequency at 1000 Hz. For describing the frequency-band correlation of the primary noise and the training signal, a frequency-band similarity ratio is defined as

$$SR = \frac{B_{\text{overlap}}}{B_{\text{primary}} + B_{\text{train}} - B_{\text{overlap}}} \quad (36)$$

where  $B_{\text{primary}}$  and  $B_{\text{train}}$  denote the bandwidths of the primary noise and training signal and  $B_{\text{overlap}}$  is the overlapped bandwidth in both the primary noise and training noise. The similarity ratio represents the similarity between the primary noise and training signal. To derive the similarity ratio between the primary noise and training noise, we first obtain their index with (33), and then compute their binary distance, as described in Appendix D.

Figure 11 shows the noise reduction levels of the different pre-trained filters. The similarity ratios on the  $x$ -axis show

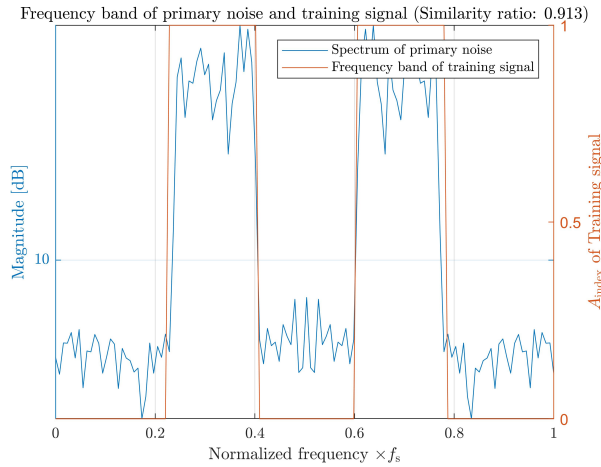


Fig. 12. The power spectrum of the primary noise, and the frequency band of the training signal of the control filter chosen by SFANC algorithm.

their similarity degrees with the controlled primary noise. The highest noise reduction is achieved as the similarity ratio approaches 1. In this case, the training signal of the control filter occupies the same spectral content as the primary noise. As the similarity ratio starts to decrease below one, the noise reduction level of the corresponding control filter also gradually reduces. For example, when  $B_{\text{train}} < B_{\text{primary}}$ , there is uncancelled disturbance remained in the error signal, which largely reduces the noise reduction performance. While  $B_{\text{train}} \geq B_{\text{primary}}$ , the error signal is mainly composed of the measurement noise. Since the power of the measurement noise is less than the disturbance, the noise reduction level degrades slower with the decreasing similarity ratio compared to the previous case. Overall a higher similarity ratio is desired to achieve a better noise cancellation.

#### B. Active control of stationary broadband noise

To train the control filters in the preliminary stage, we synthesize 88 band-limited white Gaussian noise tracks. The lower-bound of the band-pass filter increases from 500 Hz to 1000 Hz at 50 Hz interval for each bandwidth of 50 Hz to 800 Hz at 100 Hz interval. Moreover, the partitioned structure in the SFANC algorithm comprises 512 filter coefficients and 4 combs. The accumulation iteration  $L$  in (30) is set to 2048, which implies that the update rate of the control filter is 2048 iterations.

In Simulation B, the primary noise is set as a band-limited noise (600 Hz to 1000 Hz) with an amplitude of 1.2. White noise is added to the reference signal as the measurement noise, and the signal-to-noise ratio (SNR) of the reference signal is set to 15.6 dB. In this case, both the SFANC and FxLMS algorithms are used to attenuate the primary noise. In the simulation, the training noise of the pre-trained filter chosen by the SFANC algorithm has a high similarity ratio of 0.913, which implies that the frequency bands of training signal and primary noise are mostly overlapped, as illustrated in Fig. 12.

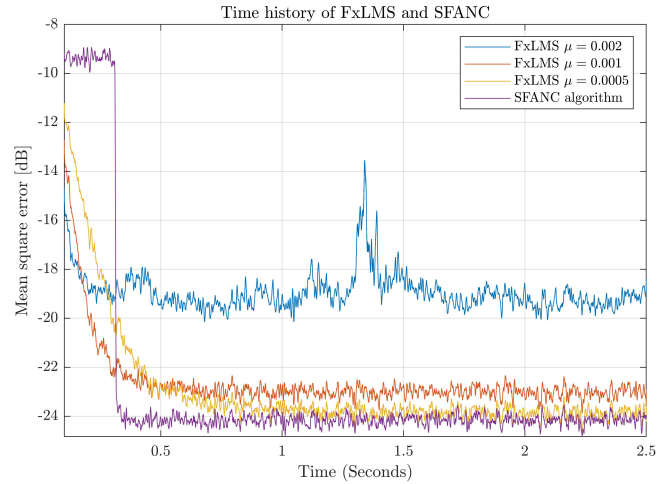


Fig. 13. The mean square error (MSE) of FxLMS and SFANC as a function of time in Simulation B. The SFANC algorithm achieves faster convergence speed and similar steady-state noise reduction performance as the FxLMS algorithm whose step size is less than 0.001. When the FxLMS algorithm chooses the step size of 0.002, it obtains a faster convergence but worse steady-state error than the SFANC algorithm.

TABLE II  
FREQUENCY BAND AND AMPLITUDE OF THE TIME-VARYING BROADBAND NOISE

Time (Second)	Frequency band (Hz)	Amplitude
0 to 3.5	500 to 850	1.5
3.5 to 7	720 to 1170	1.2
7 to 10.5	620 to 870	0.8

Figure 13 illustrates the mean square error (MSE) of the FxLMS and SFANC algorithms as a function of time. The FxLMS algorithm is executed with a 512-tap FIR adaptive filter and three different step sizes. In the simulation, the SFANC algorithm has a faster convergence speed and a similar steady-state performance as the FxLMS when the step size is less than 0.001. In contrast, the FxLMS algorithm converges faster but exhibits poorer steady-state performance as the step size increases. The steady-state noise reduction levels of three FxLMS algorithms are 9.5 dB, 13.5 dB, and 14.5 dB, respectively, whereas the SFANC algorithm achieves a noise reduction level of 14.3 dB. Therefore, as long as a high similarity ratio is obtained, the SFANC algorithm can attenuate stationary broadband noise satisfactorily with a high convergence rate.

#### C. Active control of time-varying broadband noise

In Simulation C, a change in the primary noise is invoked every 3.5 seconds, as shown in Table II. Taking reference from Simulation B, two step sizes, 0.001 and 0.0005, are adopted for the FxLMS algorithm. Upon detecting a change in the primary noise, the SFANC algorithm switches to the control filter with the highest similarity ratio while the FxLMS adapts and converges to a new steady-state error, as shown in Fig. 14. The similarity ratios between the training noises of these filters and the primary noise are 0.78, 0.89, and 0.83, respectively. The time history in Fig. 14 reveals that the SFANC algorithm reacts in a similar fashion to the conventional FxLMS algorithm.

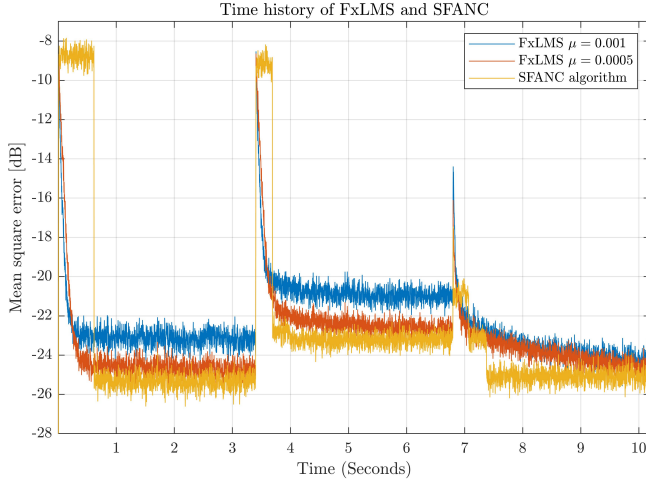


Fig. 14. The time history of the FxLMS and SFANC algorithms when dealing with the varying primary noise in Simulation C. The primary noise changes every 3.5 seconds. An updated control filter is invoked by the SFANC algorithm upon the onset of a different disturbance.

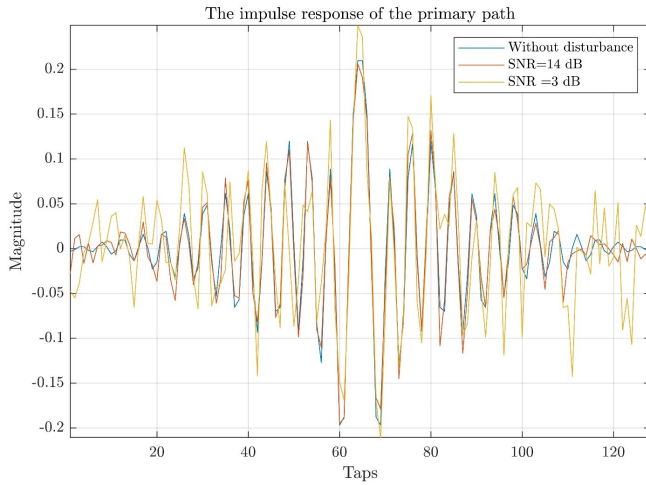


Fig. 15. Impulse responses of the primary path with different additional noises.

#### D. Active control of time-varying primary path

To verify the noise reduction performance of SFANC for the variable primary path, we add the additional noise to the primary path during the active control progress, as shown in Fig. 15. In this simulation, FxLMS with different step sizes and SFANC are utilized to deal with the varied primary path. The curves of the mean square errors of these algorithms are shown in Fig. 16. During the first five seconds, there is not any variation in the primary path, and thus, three algorithms successfully cancel the disturbance. In the second five seconds, Gaussian white noise is involved in the primary path, and the signal (the weights of the impulse response) to noise ratio (SNR) is set to 13 dB. In this case, two FxLMS algorithms achieve better noise reduction levels, while the noise reduction level of the SFANC algorithm degrades. When SNR of the primary path decreases to 3 dB in the final five seconds, the FxLMS algorithm with the bigger step size diverges. In contrast, the SFANC algorithm still maintains the noise

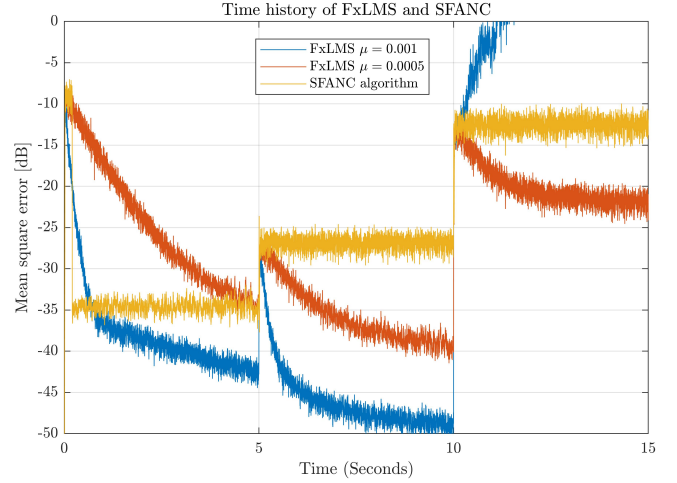


Fig. 16. Time history of the FxLMS ( $\mu = 0.001$  and  $\mu = 0.0005$ ) and SFANC algorithms for the variable primary path in Simulation E. In the first five seconds, there is no disturbance in the primary path. In the next five seconds, the Gaussian white noise is added into the impulse response of the primary path (SNR = 13 dB). In the final five seconds, the SNR of the primary path varies to 3 dB.

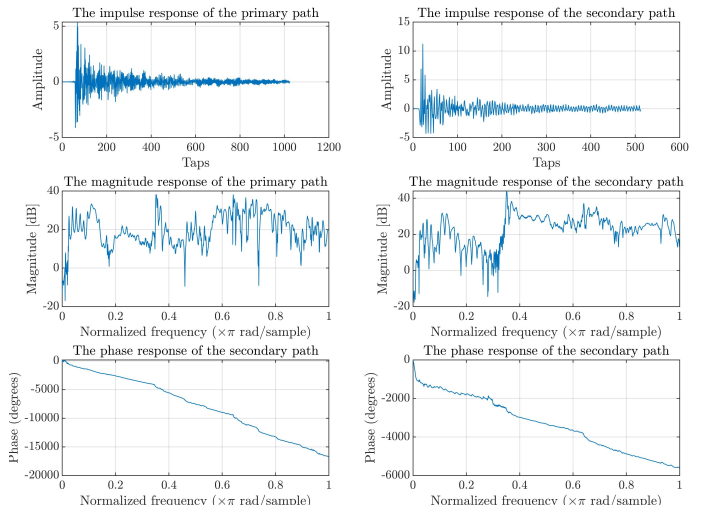


Fig. 17. The impulse responses, magnitude responses, and phase responses of the primary and secondary paths, which are measured from a noise air duct.

reduction level to some extent. The result shows the robustness of the SFANC algorithm on the slight variation of the primary path.

#### E. Active control of recorded real-world noise on the measurement primary and secondary paths

To further investigate the behavior of SFANC under a realistic scenario, a vehicle-pass-by noise is chosen as the primary noise, whose frequency ranges from 100 Hz to 8000 Hz. The primary and secondary paths are measured from an air duct, and their impulse, magnitude, and phase responses are shown in Fig. 17. The FxLMS and SFANC algorithms are used to cancel this raw noise at a sampling rate of 16000 Hz. The control filter and secondary path estimate of FxLMS have 1024 and 512 taps, and the step size is 0.001. The SFANC algorithm has a control filter with 1024 taps and two combs.

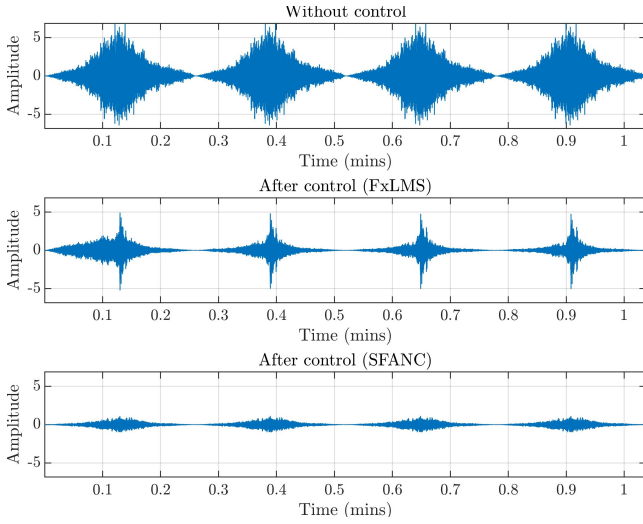


Fig. 18. From top to bottom, the disturbance: without control, after control with FxLMS, and after control with SFANC. The SFANC algorithm shows a faster convergence speed when dealing with the vehicle-pass-by sound than the FxLMS algorithm, without a specific step size selection strategy.

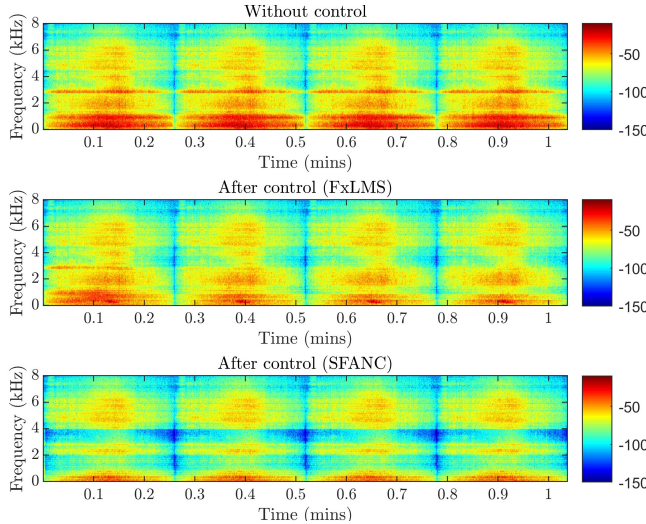


Fig. 19. From top to bottom, the spectrogram of the disturbance: without control, after control with FxLMS, and after control with SFANC.

The coefficient library of the SFANC algorithm comprises 45 control filters, which are pre-trained by different band-limited noise tracks. These tracks come from a white Gaussian noise filtered by a series of band-pass filters. The lower-bound of the band-pass filters increases from 100 Hz to 3900 Hz at 400 Hz interval for each bandwidth of 400 Hz to 3900 Hz at 400 Hz interval.

It is immediately apparent that the SFANC algorithm maintains a lower steady-state error than FxLMS, even with a time-varying disturbance, as illustrated in Fig. 18. The noise reduction levels of the SFANC and FxLMS algorithms are 15.8 dB and 5.8 dB, respectively. Fig. 19 shows the spectrograms of the noise without control, and after control by FxLMS and SFANC. It is evident that SFANC performs a better noise cancellation than FxLMS at low frequency, where the main acoustic power of the noise lies.

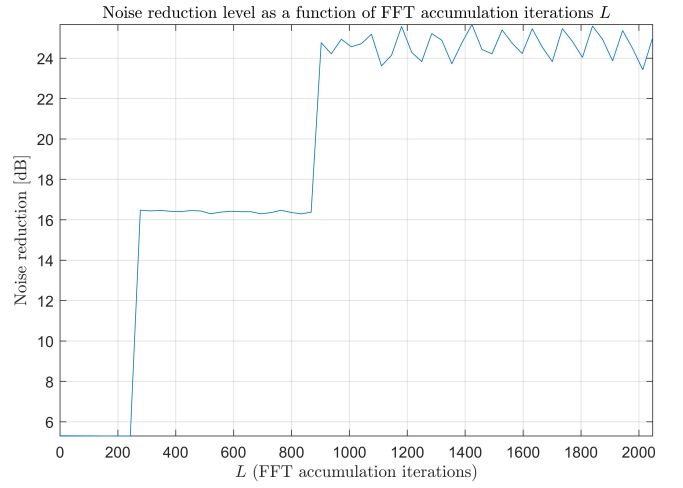


Fig. 20. Noise reduction level as a function of FFT accumulation iterations  $L$  of the SFANC algorithm in Simulation E. A small value of  $L$  ( $L < 900$ ) results in the degradation of the noise reduction performance.

Furthermore, since the convergence duration of the FxLMS algorithm is related to the variation in the power of the primary noise, the high power of the vehicle noise results in longer convergence time. In contrast, the convergence time of the SFANC algorithm is independent of the primary noise. Without using the step size to control the learning rate under different input powers, the SFANC algorithm only takes  $L = 2048$  iterations to select the suitable filter and updates to the new control filter. Subsequently, the coefficients of the control filter remain unchanged during the  $L$  iterations, which avoids the instability of adaptive updating. Therefore, the presented simulations support the feasibility of the SFANC algorithm in real-world applications.

#### F. The effect of FFT accumulation over $L$ iterations on the noise reduction performance

The accumulation over  $L$  iterations in (30) determines the rate at which the SFANC algorithm updates the coefficients of the control filter. To determine  $L$  in Simulation D, we compute the noise reduction level as a function of  $L$ , as illustrated in Fig. 20. As  $L$  increases, the noise reduction level approaches its peak. Instinctively, a small  $L$  ( $L < 900$  in this case) leads to a fast response time of the SFANC algorithm to the detected primary noise. This comes at the expense of increased variance in the periodogram of the detected primary noise, which deteriorates the noise reduction. In contrast, a large  $L$  ( $L \geq 900$  in this case) increases the accuracy of the periodogram at the expense of the response time. Therefore, in practice, a relatively large  $L$  should be chosen to ensure sufficient noise reduction while maintaining a satisfactory response time. At the moment, the optimal  $L$  has to be determined by trial and error.

## VII. CONCLUSION

Selective fixed-filter active noise control (SFANC) is an efficient approach to alleviate the computational complexity of the adaptive algorithms used in active noise control applications.

The distinct feature of this approach lies in its preliminary training stage, in which a series of control filters are pre-trained for different types of noise.

SFANC selects the most suitable pre-trained filter as the control filter. However, the challenge of this approach is the computational complexity of the control filter selection process. The paper proposes a classification scheme for the SFANC algorithm, which adopts the frequency-band-match method to choose a control filter. In this method, the pre-training noise of the selected control filter has similar spectral contents to the detected primary noise. Furthermore, the frequency-domain analysis revealed that the SFANC algorithm with this selection strategy could achieve a comparable noise reduction level as the conventional adaptive filter.

For online control, the comb-partitioning filter technique is integrated into SFANC and hence, further reduces the computational complexity in the Fourier transformation. The proposed classifier of the algorithm significantly reduces the storage requirements of the control filters and alleviates the computational load in the filter selection. Therefore, compared to the conventional adaptive algorithm used in ANC, the SFANC algorithm reduces computational complexity with a satisfactory noise reduction performance. Since the SFANC algorithm does not require adaptive feedback, unlike the conventional FxLMS algorithm, its response time, stability, and steady-state noise reduction performance is unaffected by the step size.

### VIII. ACKNOWLEDGMENTS

This research is supported by the Singapore Ministry of National Development and the National Research Foundation, Prime Minister's Office under the Cities of Tomorrow (CoT) Research Programme (CoT Award No. COT-V4-2019-1). Any opinions, findings, and conclusions or recommendations expressed in this material are those of the author(s) and do not reflect the views of the Singapore Ministry of National Development and National Research Foundation, Prime Minister's Office, Singapore.

### APPENDIX A

#### OPTIMAL CONTROL FILTER OUT THE FREQUENCY BAND

In the FxLMS algorithm, the  $k$ th recursive update equation is given by

$$\mathbf{w}(k+1) = \mathbf{w}(k) + \mu e(k) \sum_{i=0}^{L_s-1} s_i \mathbf{x}(k-i) \in \mathbb{R}^{N \times 1} \quad (\text{A.1})$$

where  $\mu$  represents the step size, and  $s_i$  denotes the  $i$ th coefficient of the secondary path model with  $L_s$  taps;  $\mathbb{R}$  and  $N$  stand for the real number and the length of the control filter, respectively. If we assume  $\mathbf{w}(0) = \mathbf{0}$ , repeating (A.1) obtains the optimal solution as

$$\mathbf{w}_o = \mu \sum_{k=0}^{\infty} e(k) \sum_{i=0}^{L_s-1} s_i \mathbf{x}(k-i) \in \mathbb{R}^{N \times 1}. \quad (\text{A.2})$$

Multiplying (A.2) by Fourier matrix

$$\mathbf{F}_N = \left( e^{-\frac{2\pi \cdot j \cdot i}{N}} / \sqrt{N} \right)_{i,j=0,\dots,N-1} \quad (\text{A.3})$$

yields

$$W_{\text{opt}}(\omega) = \mu \sum_{k=0}^{\infty} e(k) \sum_{i=0}^{L_s-1} s_i X(\omega) \in \mathbb{C}^{N \times 1} \quad (\text{A.4})$$

where  $\mathbb{C}$  denotes the complex number. Therefore, if

$$X(\omega) = 0, |\omega| \in [0, \omega_0 - B_0) \cup (\omega_0 + B_0, \pi] \quad (\text{A.5})$$

substituting (A.5) into (A.4) yields

$$W_{\text{opt}}(\omega) = 0, |\omega| \in [0, \omega_0 - B_0) \cup (\omega_0 + B_0, \pi]. \quad (\text{A.6})$$

### APPENDIX B POWER SPECTRAL DENSITY OF THE RESIDUAL ERROR

This section aims to derive the power spectral density of the residual error in (14). Since the disturbance and reference are energy signal, the auto-correlation function of (14) is derived as

$$\begin{aligned} r_e(n) &= \lim_{N \rightarrow \infty} \frac{1}{2N+1} \sum_{k=-N}^N e(k)e(k-n) \\ &= r_{d_1}(n) - r_{r_1 d_1}(n) * w_{\text{opt}}^0(n) - r_{d_1 r_1}(n) \\ &\quad * w_{\text{opt}}^0(-n) + r_{r_1}(n) * w_{\text{opt}}^0(-n) * w_{\text{opt}}^0(n) \\ &\quad + r_v(n) * w_{\text{opt}}^0(-n) * s(-n) * w_{\text{opt}}^0(n) * s(n) \end{aligned} \quad (\text{B.1})$$

where

$$r_{d_1}(n) = \lim_{N \rightarrow \infty} \frac{1}{2N+1} \sum_{k=-N}^N d_1(k)d_1(k-n) \quad (\text{B.2})$$

$$r_{r_1}(n) = \lim_{N \rightarrow \infty} \frac{1}{2N+1} \sum_{k=-N}^N r_1(k)r_1(k-n) \quad (\text{B.3})$$

$$r_{d_1 r_1}(n) = \lim_{N \rightarrow \infty} \frac{1}{2N+1} \sum_{k=-N}^N d_1(k)r_1(k-n) \quad (\text{B.4})$$

$$r_{r_1 d_1}(n) = \lim_{N \rightarrow \infty} \frac{1}{2N+1} \sum_{k=-N}^N r_1(k)d_1(k-n) \quad (\text{B.5})$$

and

$$r_v(n) = \lim_{N \rightarrow \infty} \frac{1}{2N+1} \sum_{k=-N}^N v(k)v(k-n). \quad (\text{B.6})$$

Hence, the PSD of (B.1) is calculated as

$$\begin{aligned} S_e(\omega) &= \sum_{n=-\infty}^{\infty} r_e(n) e^{-j\omega n} \\ &= S_{d_1}(\omega) - S_{r_1 d_1}(\omega) W_{\text{opt}}^0(\omega) - S_{d_1 r_1}(\omega) W_{\text{opt}}^0(-\omega) \\ &\quad + S_{r_1}(\omega) |W_{\text{opt}}^0(\omega)|^2 + S_v(\omega) |W_{\text{opt}}^0(\omega) S(\omega)|^2 \end{aligned} \quad (\text{B.7})$$

Substituting (9) and (12) into (B.7) yields

$$\begin{aligned} S_e(\omega) &= S_{d_1}(\omega) - S_{r_1 d_1}(\omega) \frac{P(\omega)}{S(\omega)} \cdot \text{rect} \left( \frac{\omega - \omega_0}{2B_0} \right) \\ &\quad + S_v(\omega) |P(\omega)|^2 \cdot \text{rect} \left( \frac{\omega - \omega_0}{2B_0} \right) \end{aligned} \quad (\text{B.8})$$

Since the PSD of the disturbance  $d_1(n)$  can be expressed as

$$\begin{aligned} S_{d_1}(\omega) &= S_{x_1}|\mathcal{P}(\omega)|^2 \cdot \text{rect}\left(\frac{\omega - \omega_0}{2B_1}\right) \\ &= S_{d_1}(\omega) \cdot \text{rect}\left(\frac{\omega - \omega_0}{2B_1}\right) \end{aligned} \quad (\text{B.9})$$

the cross-spectral density of the disturbance and filtered reference signals is stated as

$$\begin{aligned} S_{r_1 d_1}(\omega) &= S_{x_1}(\omega)\mathcal{P}^*(\omega)S(\omega) \cdot \text{rect}\left(\frac{\omega - \omega_0}{2B_1}\right) \\ &= S_{d_1 r_1}^*(\omega) \cdot \text{rect}\left(\frac{\omega - \omega_0}{2B_1}\right) \end{aligned} \quad (\text{B.10})$$

and the PSD of the noise  $v(n)$  is given by

$$S_v(\omega) = \frac{N_0}{2} \quad (\text{B.11})$$

substituting (12), (B.9), (B.10), and (B.11) into (B.8) yields

$$\begin{aligned} S_e(\omega) &= \left[ S_{d_1}(\omega) - \frac{|S_{d_1 r_1}(\omega)|^2}{S_{r_1}(\omega)} \right] \cdot \text{rect}\left(\frac{\omega - \omega_0}{2B_1}\right) \\ &\quad + \frac{N_0}{2}|\mathcal{P}(\omega)|^2 \cdot \text{rect}\left(\frac{\omega - \omega_0}{2B_0}\right). \end{aligned} \quad (\text{B.12})$$

By split the second term of the right side of (B.12), it can be rewritten as

$$\begin{aligned} S_e(\omega) &= \left[ S_{d_1}(\omega) - \frac{|S_{d_1 r_1}(\omega)|^2}{S_{r_1}(\omega)} + \frac{N_0}{2}|\mathcal{P}(\omega)|^2 \right] \\ &\quad \cdot \text{rect}\left(\frac{\omega - \omega_0}{2B_1}\right) + \frac{N_0}{2}|\mathcal{P}(\omega)|^2 \\ &\quad \cdot \left[ \text{rect}\left(\frac{\omega - \omega_0}{2B_0}\right) - \text{rect}\left(\frac{\omega - \omega_0}{2B_1}\right) \right]. \end{aligned} \quad (\text{B.13})$$

### APPENDIX C THE FILTERED REFERENCE COMB-PARTITIONING FREQUENCY DOMAIN ADAPTIVE FILTER

This section introduces how to derive the update equation of the FxCFDAF algorithm. The residual error in Fig. 4 is expressed as

$$e(k) = d(k) - \sum_{i=0}^{L_s-1} s_i \mathbf{w}^T(k-i) \mathbf{x}(k-i) \quad (\text{C.1})$$

where  $s_i$  denotes the  $i$ th weight of the secondary path, which has  $L_s$  taps, and the reference signal vector is given by

$$\mathbf{x}(k) = [x(k), x(k-1), \dots, x(k-N+1)]^T. \quad (\text{C.2})$$

The control filter is given by

$$\mathbf{w}(k) = [w_0(k), w_1(k), \dots, w_{N-1}(k)]^T. \quad (\text{C.3})$$

We separate the inner product between the control filter vector and the reference signal vector in (C.1) to  $K$  parts as

$$\begin{aligned} e(k) &= d(k) - \sum_{i=0}^{L_s-1} s_i \sum_{j=0}^{K-1} \mathbf{w}_j^T(k-i) \mathbf{x}^c(k-j-i) \\ &= d(k) - \left[ \sum_{i=0}^{L_s-1} s_i \sum_{j=0}^{K-1} \mathbf{w}_j^T(k-i) \mathbf{x}^c(k-j-i) \right]^* \end{aligned} \quad (\text{C.4})$$

where  $*$  denotes the conjugation, and

$$\mathbf{w}_j(k) = [w_j(k), w_{j+K}(k), \dots, w_{j+(M-1)K}(k)]^T. \quad (\text{C.5})$$

Inserting  $\mathbf{F}_M^{-1} \mathbf{F}_M = \mathbf{I}_M$  into (C.4) yields

$$\begin{aligned} e(k) &= d(k) - \\ &\quad \left[ \sum_{i=0}^{L_s-1} s_i \sum_{j=0}^{K-1} \mathbf{w}_j^T(k-i) \mathbf{F}_M^{-1} \mathbf{F}_M \mathbf{x}^c(k-j-i) \right]^* \\ &= d(k) - \\ &\quad \left[ \sum_{i=0}^{L_s-1} s_i \sum_{j=0}^{K-1} [\mathbf{F}_M^{-1} \mathbf{w}_j(k-i)]^T \mathbf{F}_M \mathbf{x}^c(k-j-i) \right]^* \\ &= d(k) - \\ &\quad \sum_{i=0}^{L_s-1} s_i \sum_{j=0}^{K-1} [\mathbf{W}_j(k-i)]^H [\mathbf{F}_M \mathbf{x}^c(k-j-i)]^* \end{aligned} \quad (\text{C.6})$$

Where  $\mathbf{F}_M$  is Fourier transform matrix given by (21). We define the cost function as the square of (C.6):

$$J(k) = e^2(k). \quad (\text{C.7})$$

The gradient of (C.7) with respect to  $\mathbf{W}_j^*(k)$  is derived to

$$\begin{aligned} \nabla J(k) &= -2e(k) \sum_{i=0}^{L_s-1} s_i [\mathbf{F}_M \mathbf{x}^c(k-j-i)]^* \\ &= -2e(k) [\mathbf{F}_M \mathbf{x}_f^c]^* \\ &= -2e(k) \mathbf{X}_f'^*(k-j). \end{aligned} \quad (\text{C.8})$$

We assume  $\mathbf{W}_j(k) = \mathbf{W}_j(k-i)$  in the slow adaptive progress. According to least mean square (LMS) method, the new control filter weight vector is given by

$$\mathbf{W}_j(k+1) = \mathbf{W}_j(k) + \mu e(k) \mathbf{X}_f'^*(k-j). \quad (\text{C.9})$$

The  $m$ th element of (C.9) is stated to

$$W_{m,j}^c(k+1) = W_{m,j}^c(k) + \mu e(k) X_m'^*(k-j). \quad (\text{C.10})$$

Combing (C.10) from  $j = 0$  to  $j = K-1$  yields

$$\mathbf{W}_m^c(k+1) = \mathbf{W}_m^c(k) + \mu e(k) \mathbf{X}_m'^*(k). \quad (\text{C.11})$$

### APPENDIX D BINARY DISTANCE OR SIMILARITY RATIO

There are two bit vectors  $x_i$  and  $x_j$  with the dimension of  $N$ . We define that  $\delta_i(n)$  denotes the value of  $n$ th element in  $x_i$ , and  $\delta_j(n)$  denotes the  $n$ th element of  $x_j$ , where  $n = 0, 1, \dots, N-1$ .

If  $\delta_i(n) = \delta_j(n) = 1$ , we describe that  $x_i$  and  $x_j$  has a 1–1 pair at the  $n$ th element; If  $\delta_i(n) = \delta_j(n) = 0$ , we describe that  $x_i$  and  $x_j$  has a 0–0 pair at the  $n$ th element; If  $\delta_i(n) \neq \delta_j(n) = 1$ , we describe that  $x_i$  and  $x_j$  has a inequality pair at the  $n$ th element.

Furthermore,  $m_0$  represents the number of 0–0 pairs in  $x_i$  and  $x_j$ ;  $m_1$  and  $m_2$  denote the numbers of 1–1 and inequality pairs. The binary distance or similarity ratio in the paper is defined as

$$d_{ij} = \frac{m_1}{m_1 + m_2} \quad (\text{D.1})$$

which is also called as Jaccard's coefficient [44] usually used in similarity measurement. Moreover, it is easy to know that  $d_{ij} \in (0, 1]$ .

For example, there are two 4-bit vectors, which are  $x_1 = 0100$  and  $x_2 = 1111$ , respectively, as show in Table III.  $m_1$  and  $m_2$  of these two bit vectors are found to be 1 and 3.

TABLE III  
THE BIT VECTOR EXPRESSIONS OF TWO 4-BIT BINARY DIGITS

4-bits	$\delta_{1/2}(0)$	$\delta_{1/2}(1)$	$\delta_{1/2}(2)$	$\delta_{1/2}(3)$
$x_1$	0	1	0	0
$x_2$	1	1	1	1

Therefore, the binary distance or similarity ratio between  $x_1$  and  $x_2$  is calculated as

$$d_{12} = \frac{1}{3+1} = 0.25. \quad (\text{D.2})$$

## REFERENCES

- [1] Y. Kajikawa, W. S. Gan, and S. M. Kuo, "Recent advances on active noise control: open issues and innovative applications," *APSIPA Transactions on Signal and Information Processing*, vol. 1, 2012.
- [2] C. N. Hansen, *Understanding active noise cancellation*. CRC Press, 1999.
- [3] S. J. Elliott and P. A. Nelson, "Active noise control," *IEEE signal processing magazine*, vol. 10, no. 4, pp. 12–35, 1993.
- [4] W. S. Gan, S. Mitra, and S. M. Kuo, "Adaptive feedback active noise control headset: implementation, evaluation and its extensions," *IEEE Transactions on Consumer Electronics*, vol. 51, no. 3, pp. 975–982, Aug 2005.
- [5] C. Y. Ho, K. K. Shyu, C. Y. Chang, and S. M. Kuo, "Integrated active noise control for open-fit hearing aids with customized filter," *Applied Acoustics*, vol. 137, pp. 1–8, 2018.
- [6] P. N. Samarasinghe, W. Zhang, and T. D. Abhayapala, "Recent advances in active noise control inside automobile cabins: Toward quieter cars," *IEEE Signal Processing Magazine*, vol. 33, no. 6, pp. 61–73, Nov 2016.
- [7] S. Elliott, "A review of active noise and vibration control in road vehicles," 2008. [Online]. Available: <https://eprints.soton.ac.uk/65371/>
- [8] R. Shoureshi and T. Knurek, "Automotive applications of a hybrid active noise and vibration control," *IEEE Control Systems Magazine*, vol. 16, no. 6, pp. 72–78, Dec 1996.
- [9] H.-S. Kim, J.-S. Hong, and J.-E. Oh, "Active noise control with the active muffler in automotive exhaust systems," *JSME International Journal Series C Mechanical Systems, Machine Elements and Manufacturing*, vol. 41, no. 2, pp. 178–183, 1998.
- [10] J. Cheer, "Active control of scattered acoustic fields: Cancellation, reproduction and cloaking," *The Journal of the Acoustical Society of America*, vol. 140, no. 3, pp. 1502–1512, 2016.
- [11] B. Lam, S. Elliott, J. Cheer, and W. S. Gan, "Physical limits on the performance of active noise control through open windows," *Applied Acoustics*, vol. 137, pp. 9–17, 2018.
- [12] Xuan Kong and S. M. Kuo, "Study of causality constraint on feedforward active noise control systems," *IEEE Transactions on Circuits and Systems II: Analog and Digital Signal Processing*, vol. 46, no. 2, pp. 183–186, Feb 1999.
- [13] L. Zhang and X. Qiu, "Causality study on a feedforward active noise control headset with different noise coming directions in free field," *Applied Acoustics*, vol. 80, pp. 36–44, 2014.
- [14] C. Shi, H. Li, D. Shi, B. Lam, and W.-S. Gan, "Understanding multiple-input multiple-output active noise control from a perspective of sampling and reconstruction," in *2017 Asia-Pacific Signal and Information Processing Association Annual Summit and Conference (APSIPA ASC)*. IEEE, 2017, pp. 124–129.
- [15] D. Shi, J. He, C. Shi, T. Murao, and W. S. Gan, "Multiple parallel branch with folding architecture for multichannel filtered-x least mean square algorithm," in *2017 IEEE International Conference on Acoustics, Speech and Signal Processing (ICASSP)*, March 2017, pp. 1188–1192.
- [16] D. Shi, C. Shi, and W. S. Gan, "A systolic FxLMS structure for implementation of feedforward active noise control on FPGA," in *Signal and Information Processing Association Annual Summit and Conference (APSIPA)*, 2016 Asia-Pacific. IEEE, 2016, pp. 1–6.
- [17] J. Lorente, M. Ferrer, M. D. Diego, and A. González, "Gpu implementation of multichannel adaptive algorithms for local active noise control," *IEEE/ACM Transactions on Audio, Speech and Language Processing (TASLP)*, vol. 22, no. 11, pp. 1624–1635, 2014.
- [18] X. Qiu, "Recent advances on active control of sound transmission through ventilation windows," in *Proceedings of the 24th International Congress on Sound and Vibration*, London, UK, 2017.
- [19] W. Chen, W. Rao, H. Min, and X. Qiu, "An active noise barrier with unidirectional secondary sources," *Applied Acoustics*, vol. 72, no. 12, pp. 969–974, 2011.
- [20] E. A. Wan, "Adjoint LMS: an efficient alternative to the filtered-x LMS and multiple error LMS algorithms," in *1996 IEEE International Conference on Acoustics, Speech, and Signal Processing Conference Proceedings*, vol. 3, May 1996, pp. 1842–1845 vol. 3.
- [21] C. Shi and Y. Kajikawa, "A partial-update minimax algorithm for practical implementation of multi-channel feedforward active noise control," in *2018 16th International Workshop on Acoustic Signal Enhancement (IWAENC)*. IEEE, 2018, pp. 1–15.
- [22] R. Ranjan, T. Murao, B. Lam, and W. S. Gan, "Selective active noise control system for open windows using sound classification," in *INTER-NOISE and NOISE-CON Congress and Conference Proceedings*, vol. 253, no. 6. Institute of Noise Control Engineering, 2016, pp. 1921–1931.
- [23] C. Shi, R. Xie, N. Jiang, H. Li, and Y. Kajikawa, "Selective virtual sensing technique for multi-channel feedforward active noise control systems," in *ICASSP 2019 - 2019 IEEE International Conference on Acoustics, Speech and Signal Processing (ICASSP)*, May 2019, pp. 8489–8493.
- [24] D. Y. Shi, B. Lam, and W. Gan, "A novel selective active noise control algorithm to overcome practical implementation issue," in *2018 IEEE International Conference on Acoustics, Speech and Signal Processing (ICASSP)*, April 2018, pp. 1130–1134.
- [25] B. Rafaely, "Active noise reducing headset-an overview," in *INTER-NOISE and NOISE-CON Congress and Conference Proceedings*, vol. 2001, no. 3. Institute of Noise Control Engineering, 2001, pp. 2144–2153.
- [26] M. Pawelczyk, "Analogue active noise control," *Applied Acoustics*, vol. 63, no. 11, pp. 1193–1213, 2002.
- [27] D. Shi, C. Shi, and W.-S. Gan, "Effect of the audio amplifier's distortion on feedforward active noise control," in *2017 Asia-Pacific Signal and Information Processing Association Annual Summit and Conference (APSIPA ASC)*. IEEE, 2017, pp. 469–473.
- [28] W. Jung, S. J. Elliott, and J. Cheer, "Local active control of road noise inside a vehicle," *Mechanical Systems and Signal Processing*, vol. 121, pp. 144–157, 2019.
- [29] Y. LeCun, Y. Bengio *et al.*, "Convolutional networks for images, speech, and time series," *The handbook of brain theory and neural networks*, vol. 3361, no. 10, p. 1995, 1995.
- [30] B. Widrow, J. R. Glover, J. M. McCool, J. Kaunitz, C. S. Williams, R. H. Hearn, J. R. Zeidler, J. Eugene Dong, and R. C. Goodlin, "Adaptive noise cancelling: Principles and applications," *Proceedings of the IEEE*, vol. 63, no. 12, pp. 1692–1716, Dec 1975.
- [31] A. V. Oppenheim, A. S. Willsky, and S. Nawab, "Signals and systems (prentice-hall signal processing series)," 1996.
- [32] B. Widrow and D. Samuel, "Streams (2005), adaptive signal processing, person education," *New Delhi*.
- [33] S. M. Kuo and D. Morgan, *Active noise control systems: algorithms and DSP implementations*. John Wiley and Sons, Inc., 1995.
- [34] S. S. Haykin, *Adaptive filter theory*. Pearson Education India, 2008.
- [35] P. C. W. Sommen, "Partitioned frequency domain adaptive filters," in *Twenty-Third Asilomar Conference on Signals, Systems and Computers, 1989*, vol. 2, Oct 1989, pp. 677–681.
- [36] P. C. W. Sommen and E. de Wilde, "Equal convergence conditions for normal- and partitioned-frequency domain adaptive filters," in *[Proceedings] ICASSP-92: 1992 IEEE International Conference on Acoustics, Speech, and Signal Processing*, vol. 4, Mar 1992, pp. 69–72 vol.4.
- [37] J. J. Shynk, "Frequency-domain and multirate adaptive filtering," *IEEE Signal Processing Magazine*, vol. 9, no. 1, pp. 14–37, Jan 1992.
- [38] X. L. S. Liu and J. Tian, "Transform domain adaptive filter in active noise control," in *6th International Conference on Signal Processing*, 2002., vol. 1, Aug 2002, pp. 272–275 vol.1.
- [39] F. Yang and J. Yang, "Optimal step-size control of the partitioned block frequency-domain adaptive filter," *IEEE Transactions on Circuits and Systems II: Express Briefs*, vol. 65, no. 6, pp. 814–818, June 2018.
- [40] F. Yang, G. Enzner, and J. Yang, "Statistical convergence analysis for optimal control of dft-domain adaptive echo canceler," *IEEE/ACM*

- Transactions on Audio, Speech, and Language Processing*, vol. 25, no. 5, pp. 1095–1106, May 2017.
- [41] F. Yang, Y. Cao, M. Wu, F. Albu, and J. Yang, “Frequency-domain filtered-x lms algorithms for active noise control: A review and new insights,” *Applied Sciences*, vol. 8, no. 11, 2018. [Online]. Available: <https://www.mdpi.com/2076-3417/8/11/2313>
- [42] P. G. Estermann, A. Kaelin, and A. G. Lindgren, “Analysis of partitioned frequency-domain lms adaptive algorithm with application to a hands-free telephone system echo canceller,” *International Journal of Adaptive Control and Signal Processing*, vol. 14, no. 6, pp. 587–608, 2000.
- [43] P. Welch, “The use of fast fourier transform for the estimation of power spectra: A method based on time averaging over short, modified periodograms,” *IEEE Transactions on Audio and Electroacoustics*, vol. 15, no. 2, pp. 70–73, June 1967.
- [44] S. Niwattanakul, J. Singthongchai, E. Naenudorn, and S. Wanapu, “Using of jaccard coefficient for keywords similarity,” in *Proceedings of the international multiconference of engineers and computer scientists*, vol. 1, no. 6, 2013, pp. 380–384.
- [45] S. S. Choi, S. H. Cha, and C. C. Tappert, “A survey of binary similarity and distance measures,” *Journal of Systemics, Cybernetics and Informatics*, vol. 8, no. 1, pp. 43–48, 2010.



**Lam Bhan** received his B.Eng. (Hons) and Ph.D. degrees in electrical and electronic engineering from Nanyang Technological Univ., Singapore, in 2013 and 2019, respectively. He is currently a research fellow at the School of Electrical and Electronic Engineering, Nanyang Technological Univ., Singapore. His current research includes the acoustics of active noise control, soundscape, and signal processing for active control



parameter estimation.

**Shulin Wen** received her B. S. degree from the School of Electronic Information and Communications, Huazhong University of Science and Technology, Wuhan, China in 2012, and the Ph.D. degree from the Institute of Acoustics, Chinese Academy of Sciences on Signal processing in 2018. She started working as a research fellow in the INFINITUS center of the Electrical and Electronics Engineering Department at Nanyang Technological University from 2018. Her research interests include active noise control, adaptive signal processing, and Bayesian



**Dongyuan Shi** received his B.ENG and M.S degrees in the University of Electronic Science and Technology of China (UESTC), in 2010 and 2013, respectively. He worked as a research fellow of the Applied Micro-fluidicology Laboratory of Nanyang Technology University to design the cell CMOS image capture system and the framework of the image processing algorithm from 2013-2014. He is currently pursuing Ph.D. degree in electrical and electronic engineering at Nanyang Technological University (NTU), Singapore. His research interests include advanced digital signal processing, adaptive array processing, high-speed real-time digital system implementation, and active noise control.



**Woon-Seng Gan** received his BEng (1st Class Hons) and PhD degrees, both in Electrical and Electronic Engineering from the University of Strathclyde, UK in 1989 and 1993 respectively. He is currently a Professor of Audio Engineering in the School of Electrical and Electronic Engineering in Nanyang Technological University. He also served as the Head of the Information Engineering Division in the School of Electrical and Electronic Engineering in Nanyang Technological University from 2011-2014. He is currently the Director, Centre for Infocomm Technology @ NTU, which was formed in 2011 and brings together expert in the area of Information and Communication Engineering.

His research has been concerned with the connections between the physical world, signal processing and sound control, which resulted in the practical demonstration and licensing of spatial audio algorithms, directional sound beam, and active noise control for headphones. He has published more than 330 international refereed journal and conference papers, and has translated his research into 6 granted US/Singapore patents. He had co-authored three books on Subband Adaptive Filtering: Theory and Implementation (John Wiley, 2009); Embedded Signal Processing with the Micro Signal Architecture, (Wiley-IEEE, 2007); and Digital Signal Processors: Architectures, Implementations, and Applications (Prentice Hall, 2005). In 2017, he won the APSIPA Sadao Furui Prize Paper Award. He is a Fellow of the Audio Engineering Society(AES), a Fellow of the Institute of Engineering and Technology(IET), and a Senior Member of the IEEE. He also served as an Associate Editor of the IEEE/ACM Transaction on Audio, Speech, and Language Processing (TASLP; 2012-15); IEEE Signal Processing Letters (SPL; 2016-2019); and Associate Technical Editor of the Journal of Audio Engineering Society (JAES; 2013-).